

## Time-averaged pressure drop induced by a jet pump in oscillatory flow

Ye Feng, Ke Tang, Tao Jin, Kaihao Zhang, and Rui Yang

Citation: *The Journal of the Acoustical Society of America* **142**, 1730 (2017); doi: 10.1121/1.5004541

View online: <https://doi.org/10.1121/1.5004541>

View Table of Contents: <https://asa.scitation.org/toc/jas/142/4>

Published by the [Acoustical Society of America](#)

---

### ARTICLES YOU MAY BE INTERESTED IN

[A thermoacoustic-Stirling heat engine: Detailed study](#)

*The Journal of the Acoustical Society of America* **107**, 3148 (2000); <https://doi.org/10.1121/1.429343>

[Numerical investigation on turbulent oscillatory flow through a jet pump](#)

*The Journal of the Acoustical Society of America* **145**, 1417 (2019); <https://doi.org/10.1121/1.5094346>

[Thermoacoustic engines](#)

*The Journal of the Acoustical Society of America* **84**, 1145 (1988); <https://doi.org/10.1121/1.396617>

[Numerical investigation on nonlinear effect and vortex formation of oscillatory flow throughout a short tube in a thermoacoustic Stirling engine](#)

*Journal of Applied Physics* **121**, 214902 (2017); <https://doi.org/10.1063/1.4984795>

[Experimental investigation of the influence of natural convection and end-effects on Rayleigh streaming in a thermoacoustic engine](#)

*The Journal of the Acoustical Society of America* **143**, 361 (2018); <https://doi.org/10.1121/1.5021331>

[A looped-tube traveling-wave engine with liquid pistons](#)

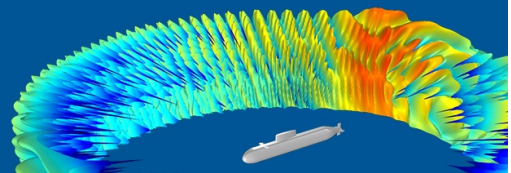
*Journal of Applied Physics* **122**, 114902 (2017); <https://doi.org/10.1063/1.4986409>

---

**COMSOL Day**  
Acoustics

*A free, online event* where you can attend  
multiphysics simulation sessions, ask  
COMSOL staff your questions, and more

JOIN US MAY 25 »



# Time-averaged pressure drop induced by a jet pump in oscillatory flow

Ye Feng,<sup>1</sup> Ke Tang,<sup>2,a)</sup> Tao Jin,<sup>2</sup> Kaihao Zhang,<sup>3</sup> and Rui Yang<sup>1</sup>

<sup>1</sup>Department of Energy Engineering, Zhejiang University, 38 Zheda Road, Hangzhou 310027, China

<sup>2</sup>Key Laboratory of Refrigeration and Cryogenic Technology of Zhejiang Province, Zhejiang University, 38 Zheda Road, Hangzhou 310027, China

<sup>3</sup>Department of Mechanical Science and Engineering, University of Illinois, 1206 West Green Street, Urbana, Illinois 61801, USA

(Received 14 May 2017; revised 23 August 2017; accepted 9 September 2017; published online 2 October 2017)

Gedeon streaming is known to considerably deteriorate the thermal efficiency of a traveling-wave thermoacoustic engine with looped configuration. The time-average pressure drop induced by a jet pump can efficiently suppress the Gedeon streaming. In this study, such suppression mechanism of the jet pump is investigated, and the emphasis is put on the effects of the dimensionless rounding, the taper angle, and the cross-sectional area ratio. An experimental apparatus has been set up to measure the time-averaged pressure drop induced by the jet pumps in oscillatory flow. Controlled experiments and characterization reveal the time-averaged pressure drop and working efficiency increase with a rise in dimensionless rounding when it is less than 0.15. For jet pumps with the fixed opening areas, the taper angle in the range from 3° to 9° is capable of producing a larger time-averaged pressure drop with a higher working efficiency, and the change of taper angle has little effect on the performance. However, performance degradation is observed as the taper angle increases beyond 9°. Moreover, when the taper angle ranges from 3° to 9°, the time-averaged pressure drop and working efficiency can be improved by increasing the cross-sectional area ratio.

© 2017 Acoustical Society of America. <https://doi.org/10.1121/1.5004541>

[JDM]

Pages: 1730–1738

## I. INTRODUCTION

Thermoacoustic effect refers to the time-averaged conversion between thermal energy and acoustic energy due to the thermal interaction between fluid and solid boundary. A thermoacoustic engine, based on thermoacoustic effect, exhibits advantages in its simple configuration and reliability without moving parts, and is environmentally friendly using natural working fluids, such as helium, nitrogen, or carbon dioxide. It also has the potential to be powered by low-grade thermal energy, which is abundantly available from the industrial heat emission, the geothermal energy, etc. There have been extensive investigations on thermoacoustic engine applications in electrical power generation,<sup>1–4</sup> refrigeration,<sup>5,6</sup> and water pumping<sup>7,8</sup> to name a few.

Compared with a standing-wave thermoacoustic engine, a traveling-wave thermoacoustic engine has a higher theoretical efficiency due to perfect thermal contact between working fluid and solid boundary in the regenerator,<sup>9</sup> thus becomes more sought-after. Traveling-wave thermoacoustic engine was first proposed by Ceperley in 1979.<sup>9</sup> In 1999, Backhaus and Swift<sup>10</sup> successfully built a thermoacoustic Stirling engine, achieving a thermal efficiency of 0.3, which promoted a rapid development of thermoacoustic engines.<sup>11–15</sup> However, a traveling-wave thermoacoustic engine usually has a loop configuration, which may cause an acoustic streaming named as Gedeon streaming.<sup>16</sup> The

Gedeon streaming is a time-averaged mass flow superimposed on an oscillatory flow, circulating throughout the looped configuration. It can also cause heat loss and severely reduces the efficiency of thermoacoustic engines.<sup>17–20</sup>

Due to the negative effect of the Gedeon streaming, a “jet pump,” proposed by Backhaus and Swift,<sup>10</sup> has been used in thermoacoustic engines to suppress the Gedeon streaming. Figure 1 shows the schematic of a typical thermoacoustic Stirling engine with a jet pump. A so-called jet pump above the main cold heat exchanger is characterized by a tapered hole with different inlet and outlet areas. The oscillatory flow in thermoacoustic engines switches its direction in each of the half time periods. As a result, the pressure drop through the jet pump becomes asymmetric between the forward and the backward flow, leading to a time-averaged pressure drop. The Gedeon streaming can be suppressed by a carefully designed time-averaged pressure drop.

The time-averaged pressure drop induced by a jet pump is usually calculated by the formula proposed by Backhaus and Swift,<sup>10,21</sup> as shown in Eq. (1). This is based on Iguchi’s hypothesis<sup>22</sup> that the oscillating fluid with large amplitude has no memory on the previous flow at any point, and the flow at each time can be seen as a quasi-static flow:

$$\Delta p_a = \frac{\rho U_{1,jp}^2}{8a_s^2} \left\{ \left[ k_{\text{exp},s} + \left( \frac{a_s}{a_b} \right)^2 k_{\text{con},b} \right] - \left[ k_{\text{con},s} + \left( \frac{a_s}{a_b} \right)^2 k_{\text{exp},b} \right] \right\}, \quad (1)$$

<sup>a)</sup>Electronic mail: ktang@zju.edu.cn

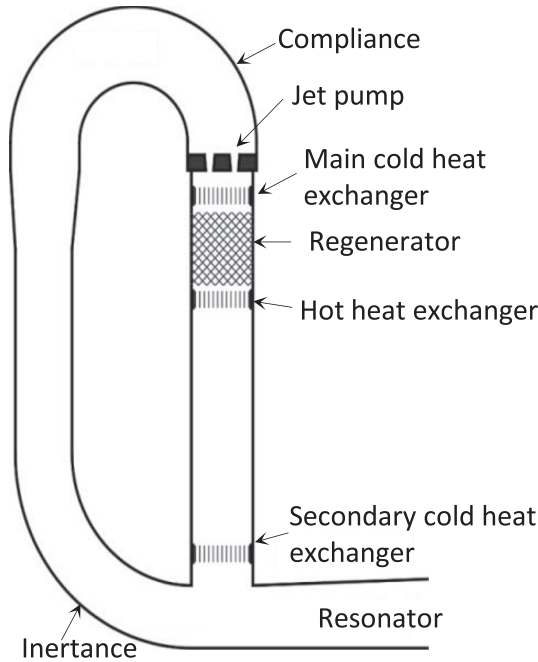


FIG. 1. Schematic of a typical thermoacoustic Stirling engine with a jet pump.

where  $\rho$  is the mean density of working fluid,  $U_{1,jp}$  is the volumetric velocity amplitude through the jet pump,  $a_s$  and  $a_b$  are the areas of small and big openings of a jet pump.  $k_{exp}$  is the expansion loss coefficient, and  $k_{exp} = 1$  when  $A_{loop} \gg a_s$  and  $a_b$  ( $A_{loop}$  is the area of pipe where the jet pump locates).  $k_{con}$  is the contraction loss coefficient, and  $k_{con} = 0.5$  when  $A_{loop} \gg a_s$  and  $a_b$  with a sharp edge.  $k_{con}$  decreases as a function of rounding radius  $r$  at the edge of channel opening.<sup>23</sup>

Nevertheless, the applicability of Iguchi's hypothesis on a jet pump is still controversial.<sup>24,25</sup> Moreover, only the asymmetry of hydrodynamic end effects is involved in Eq. (1), but the other factors of the channel, which may affect the performance, lack discussion. In our previous numerical simulation studies,<sup>26</sup> we discovered that the rounding radius at the edge of the small opening and the taper angle show significant impact on the jet pump's performance.

In order to systematically study the resistance characteristics of the jet pump in oscillatory flow, an experimental apparatus has been set up to analyze the time-averaged pressure drop induced by the jet pump and its dependence on the jet pump's configurations, including the dimensionless rounding at the edge of the small opening, the taper angle, and the cross-sectional area ratio, as well as its working efficiency to suppress the Gedeon streaming.

## II. EXPERIMENTAL APPARATUS AND DATA REDUCTION

### A. Experimental apparatus

Figure 2 is a schematic of the experimental apparatus used to investigate the jet pump's performance. The experimental apparatus consists of a linear compressor, a tested jet pump, a particle packing chamber, and a reservoir. The tested jet pump is a stainless steel cylinder with a tapered

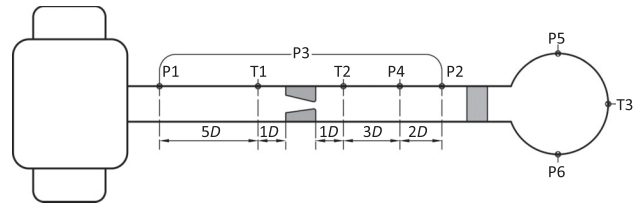


FIG. 2. Schematic of the experimental apparatus.

hole, as shown in Fig. 3. The main dimensions are tabulated in Table I. For all samples, the diameter of the small opening  $d_s$  is 7 mm (the diameter of the smallest cross section). The surface roughness,  $R_a$ , at which the flow reaches the highest velocity in the jet pump is  $1.6 \mu\text{m}$ , and it is smaller than the viscous penetration depth  $\delta_\nu$  (approximately  $53 \mu\text{m}$ ). The dimensionless rounding at the edge of small opening  $r/d_s$  is defined as the ratio of rounding radius to diameter of the small opening. The cross-sectional area ratio  $a_b/a_s$  is defined as the area ratio of the big opening  $a_b$  to the small opening  $a_s$ . Nitrogen gas, at a pressure of 3 MPa, is used as the working fluid in the experiment, and the frequency of the oscillatory flow is 60 Hz.

A resistance-and-compliance (RC) load, which is usually used for measuring the acoustic power output of thermoacoustic engines,<sup>10,27</sup> is adopted to characterize the velocity amplitude through the jet pump. The RC load often takes the form of a needle valve combined with a reservoir. The opening of the needle valve is very small, which may affect the flow field inside the pipe substantially. Here, the particle packing instead of the needle valve is used to provide resistance in our experimental apparatus. The jacket of the particle packing chamber is cooled by water to prevent the overheating, especially for the case with large velocity. The volume of reservoir  $V_{res}$  is 1 liter.

Six pressure sensors and three thermometers are arranged in the system as shown in Fig. 2. The pressure sensors P1 and P2 of model 113B28 (PCB PIEZOTRONICS Inc., Depew, New York) are located at a same distance of  $6D$  (the diameter of the pipe  $D$  is 28 mm) on each side of the jet pump to measure the dynamic pressure, with an accuracy of 3.447 kPa. The pressure drop of the working gas is measured by a two-way differential pressure sensors P3, with the range from  $-200$  to  $200$  kPa and the accuracy of 0.2% FS. The pressure sensors P4 and P5 are used to measure the mean pressure in the pipe and the reservoir, with the range of 0–5 MPa and the accuracy of 0.2% FS. Since the pressure

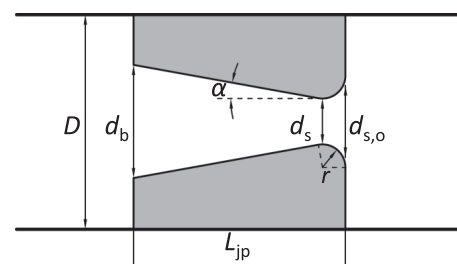


FIG. 3. Schematic of the jet pump.

TABLE I. Main dimensions of the jet pump.

No.	$r/d_s$	$\alpha$ (°)	$L_{jp}$ (mm)	$d_b$ (mm)	$d_{s,o}$ (mm)	No.	$r/d_s$	$\alpha$ (°)	$L_{jp}$ (mm)	$d_b$ (mm)	$d_{s,o}$ (mm)
1	0	5	19.3	10.4	7	12	0.3	12	9.4	10	11.2
2	0.05	5	19.3	10.3	7.7	13	0.3	15	8.0	10	11.2
3	0.08	5	19.3	10.3	8.1	14	0.3	20	6.6	10	11.2
4	0.12	5	19.3	10.2	8.7	15	0.3	5	7	7.8	11.2
5	0.15	5	19.3	10.2	9.1	16	0.3	5	10.5	8.4	11.2
6	0.2	5	19.3	10.1	9.8	17	0.3	5	14	9.1	11.2
7	0.25	5	19.3	10.1	10.5	18	0.3	5	28	11.5	11.2
8	0.3	5	19.3	10	11.2	19	0.3	9	7	8.5	11.2
9	0.3	3	30.8	10	11.2	20	0.3	9	11.7	10	11.2
10	0.3	7	14.4	10	11.2	21	0.3	9	14	10.7	11.2
11	0.3	9	11.7	10	11.2	22	0.3	9	22.4	13.4	11.2

amplitude in the reservoir is much smaller than that in the pipe, the pressure sensor P6 of model 106B manufactured by PCB PIEZOTRONICS Inc., with an accuracy of 0.57 kPa, is used to measure the dynamic pressure in the reservoir. The temperatures of the working gas at each end of the jet pump, as well as that in the reservoir, are measured by three sheathed PT100 platinum resistance thermometers (i.e., T1, T2, and T3), with accuracies of  $\pm 0.1$  °C.

## B. Data reduction

The pressure drop of oscillatory flow through the jet pump can be expressed as

$$\Delta p(t) = \frac{1}{2} \rho k u(t) |u(t)| + \rho \int_0^{L_{jp}} \frac{du(t)}{dt} dx, \quad (2)$$

where  $u(t)$  is the instantaneous velocity through the small opening of the jet pump. The second item on the right-hand side of Eq. (2) presents the inertial effect of jet pump. The velocity is assumed to be sinusoidal

$$u(t) = u_1 \sin \omega t, \quad (3)$$

where  $u_1$  is the velocity amplitude through the small opening of jet pump, and  $\omega$  is the angular frequency. The time-averaged pressure drop and the acoustic power loss are

$$\Delta p_a = \int_0^T \Delta p(t) dt / T, \quad (4)$$

$$\Delta E = \int_0^T \Delta p(t) U_{1,jp}(t) dt / T, \quad (5)$$

where  $T$  is the time period.

It is assumed that the resistance coefficient of the working gas through the jet pump in a direction during their half time periods is constant. Since  $u$  is a periodic function, the integral over a cycle of the second item on the right-hand side of Eq. (2) will vanish, therefore the inertance effect of the jet pump can be ignored here. Substituting Eqs. (2) and (3) into Eqs. (4) and (5), the time-averaged pressure drop and the acoustic power loss can be rewritten as

$$\begin{aligned} \Delta p_a &= \left( \int_0^{T/2} \frac{1}{2} k_+ \rho u_1^2 \sin^2 \omega t dt - \int_{T/2}^T \frac{1}{2} k_- \rho u_1^2 \sin^2 \omega t dt \right) / T \\ &= \frac{1}{8} \rho u_1^2 (k_+ - k_-), \end{aligned} \quad (6)$$

$$\begin{aligned} \Delta E &= \left( \int_0^{T/2} \frac{1}{2} k_+ a_s \rho u_1^3 \sin^3 \omega t dt - \int_{T/2}^T \frac{1}{2} k_- a_s \rho u_1^3 \sin^3 \omega t dt \right) / T \\ &= \frac{a_s}{3\pi} \rho u_1^3 (k_+ + k_-), \end{aligned} \quad (7)$$

where the  $k_+$  represents the resistance coefficient of forward fluid flow, i.e., the flow in the converging direction, while the  $k_-$  means the resistance coefficient of backward fluid flow, i.e., the flow in the diverging direction.

According to Eqs. (6) and (7),  $k_+$  and  $k_-$  can be calculated by

$$k_+ = \frac{3\pi \Delta E + 8 \Delta p_a a_s u_1}{2 \rho u_1^3 a_s}, \quad (8)$$

$$k_- = \frac{3\pi \Delta E - 8 \Delta p_a a_s u_1}{2 \rho u_1^3 a_s}. \quad (9)$$

In order to evaluate the performance of a jet pump, three parameters, i.e., the coefficient of time-averaged resistance  $k_a$ , the coefficient of overall resistance  $k_{total}$ , and the coefficient of effectiveness  $\varepsilon$ , were proposed in our former work to characterize the ability of the jet pump inducing time-averaged pressure drop.<sup>26</sup> The definitions are as follows:

$$k_a = \frac{\int_0^T \Delta p dt}{\int_0^T \frac{\rho u^2}{2} dt} = \frac{\int_0^{T/2} \frac{\rho u^2}{2} k_+ dt - \int_{T/2}^T \frac{\rho u^2}{2} k_- dt}{\frac{1}{4} \rho u_1^2 T} = \frac{k_+ - k_-}{2}, \quad (10)$$

$$k_{\text{total}} = \frac{\int_0^T |\Delta p| dt}{\int_0^T \frac{\rho u^2}{2} dt} = \frac{\int_0^{T/2} \frac{\rho u^2}{2} k_+ dt + \int_{T/2}^T \frac{\rho u^2}{2} k_- dt}{\frac{1}{4} \rho u_1^2 T} = \frac{k_+ + k_-}{2}, \quad (11)$$

$$\varepsilon = \left| \frac{\Delta p_a}{\Delta E} \right|. \quad (12)$$

The coefficient of time-averaged resistance  $k_a$  corresponds to the time-averaged pressure drop  $\Delta p_a$ , whereas the coefficient of overall resistance  $k_{\text{total}}$  corresponds to the total pressure loss  $\Delta p_{\text{total}}$ . The coefficient of effectiveness  $\varepsilon$  denotes the time-averaged pressure drop obtained from unit fluid flow power consumption. In the light of these, a larger  $k_a$  means that a jet pump has the higher potential to produce the time-averaged pressure drop. A larger  $k_{\text{total}}$  implies that a jet pump will cause the larger overall pressure loss. A jet pump with a higher  $\varepsilon$  can produce a larger time-averaged pressure drop with a given flow power consumption, i.e., a higher working efficiency.

Substituting Eqs. (8) and (9) into Eqs. (10) and (11) gives

$$k_a = \frac{4\Delta p_a}{\rho u_1^2}, \quad (13)$$

$$k_{\text{total}} = \frac{3\pi\Delta E}{2a_s \rho u_1^3}. \quad (14)$$

Based on Eqs. (13) and (14), Eq. (12) can be written as

$$\varepsilon = \left| \frac{3\pi k_a}{8u_1 a_s k_{\text{total}}} \right|. \quad (15)$$

The jet pump with the maximum theoretical working efficiency would have the minor resistance coefficient  $k_{\text{min}} = 0$ . Thus, the maximum theoretical coefficient of effectiveness  $\varepsilon_{\text{max}}$  can be calculated by

$$\varepsilon_{\text{max}} = \frac{3\pi}{8u_1 a_s}. \quad (16)$$

Based on the analogy of acoustics and electrics,<sup>10</sup>  $u_1$  can be calculated by

$$u_1 = \frac{U_{1,\text{jp}}}{a_s} = \rho_{\text{res}} \frac{i\omega C_{\text{res}} p_{1,\text{res}} + i\omega C_2 p_{1,2}}{\rho_{\text{jp}} a_s} = \rho_{\text{res}} \frac{i\omega V_{\text{res}} p_{1,\text{res}} / p_{m,\text{res}} + i\omega V_2 p_{1,2} / p_{m,\text{pi}}}{\gamma \rho_{\text{jp}} a_s}, \quad (17)$$

where  $C_{\text{res}}$  and  $C_2$  denote acoustic compliances of the reservoir and the pipe between the reservoir and the jet pump, respectively.  $p_{1,\text{res}}$  and  $p_{1,2}$  are the pressure amplitudes in the reservoir and in the pipe behind the jet pump, measured by P6 and P2, respectively.  $V_2$  is the volume of the pipe between the reservoir and jet pump.  $p_{m,\text{res}}$  and  $p_{m,\text{pi}}$  are the mean operating pressures in the reservoir and in the pipe, measured by P5 and P4, respectively.  $\gamma$  is the specific heat

capacity ratio of the working fluid.  $\rho_{\text{res}}$  and  $\rho_{\text{jp}}$  are the densities of fluid in the reservoir and in the jet pump, respectively.

The time-averaged pressure drop  $\Delta p_a$  can be measured by P3. The acoustic power loss  $\Delta E$  can be calculated by

$$\Delta E = \frac{1}{2} \text{Re}(p_{1,1} \tilde{U}_{1,1}) - \frac{1}{2} \text{Re}(p_{1,2} \tilde{U}_{1,2}), \quad (18)$$

where  $p_{1,1}$  is the pressure amplitude in the pipe before the jet pump measured by P1.  $U_{1,1}$  and  $U_{1,2}$  are the volumetric velocity amplitudes on each side of the jet pump, respectively. The diacritical mark  $\sim$  stands for complex conjugate. Since the viscosity loss in the pipe is much less than the local resistance loss of the jet pump, the impact of the acoustic power loss in pipe is omitted. The volumetric velocity amplitudes on each side of the jet pump  $U_{1,1}$  and  $U_{1,2}$  can be calculated by

$$U_{1,1} = U_{1,\text{jp}} - \rho_{\text{res}} \frac{i\omega C_1 p_{1,1}}{\rho_{\text{jp}}} = \frac{i\omega V_{\text{res}} p_{1,\text{res}} \rho_{\text{res}}}{\gamma \rho_{\text{jp}} p_{m,\text{res}}} + i\omega \rho_{\text{res}} \frac{V_2 p_{1,2} - V_1 p_{1,1}}{\gamma \rho_{\text{jp}} p_{m,\text{pi}}}, \quad (19)$$

$$U_{1,2} = \rho_{\text{res}} \frac{U_{1,\text{res}} - i\omega C_3 p_{1,2}}{\rho_{\text{jp}}} = \frac{i\omega V_{\text{res}} \rho_{\text{res}} p_{1,\text{res}}}{\gamma \rho_{\text{jp}} p_{m,\text{res}}} - \frac{i\omega \rho_{\text{res}} V_3 p_{1,2}}{\gamma \rho_{\text{jp}} p_{m,\text{pi}}}, \quad (20)$$

where  $C_1$  and  $V_1$  are the acoustic compliance and the volume of connecting pipe between P1 and jet pump, respectively.  $C_3$  and  $V_3$  denote the acoustic compliance and the volume of connecting pipe between P2 and reservoir, respectively.

For oscillatory flow, Reynolds number can be defined as<sup>28</sup>

$$\text{Re} = \frac{u_1 \delta_\nu \rho}{\mu}, \quad (21)$$

where  $\mu$  is the viscosity of the working fluid. In this study, Re ranges from  $2 \times 10^3$  to  $8 \times 10^3$ , which corresponds to the velocity amplitude through the pipe  $u_{1,\text{p}}$  within the range from 1.25 to 5 m/s. Using the definition of Re, the maximum theoretical coefficient of effectiveness  $\varepsilon_{\text{max}}$  can be written as

$$\varepsilon_{\text{max}} = \frac{3\pi \delta_\nu \rho}{8 \text{Re} \mu a_s}. \quad (22)$$

The values of maximum theoretical coefficient of effectiveness  $\varepsilon_{\text{max}}$  for different Re are shown in Table II. In addition, the pressure amplitudes at the opening of a jet pump closed to reservoir  $p_{1,2f}$ , and the phase differences between that pressure and velocity through the jet pump  $ph(p_{1,2f}) - ph(u_1)$  for different Re are also listed in Table II. Based on the study of Ohmi and Iguchi,<sup>29</sup> the oscillatory flow transforms to turbulence when Re is larger than the critical value  $\text{Re}_c = 305(d/\delta_\nu)^{1/7}$ . In our experiment, Re is always beyond  $\text{Re}_c$ , indicating that these measurements are in the turbulent regime where numerical simulations of oscillatory flow are unreliable. Therefore, measurements in this regime of flow,

TABLE II. The operation parameters and maximum theoretical coefficient of effectiveness  $\varepsilon_{\max}$  for different Re.

Re	$2 \times 10^3$	$4 \times 10^3$	$6 \times 10^3$	$7 \times 10^3$	$8 \times 10^3$
$p_{1,2f}$ (kPa)	13.7	42.7	76.6	97.2	111.7
$ph(p_{1,2f}) - ph(u_1)$ (°)	-14.7	-22.6	-28.4	-31.1	-33.1
$\varepsilon_{\max}$ (kPa/W)	1.52	0.76	0.51	0.43	0.38

which is of the most interest to thermoacoustic engine, are essential.

### III. EXPERIMENTAL RESULTS AND DISCUSSION

#### A. Effect of dimensionless rounding

The dependences of  $k_+$  and  $k_-$  on dimensionless rounding  $r/d_s$  are shown in Fig. 4 (No. 1–8 in Table I). Rounding at the edge of the small opening has more prominent effect on  $k_-$  compared with that on  $k_+$ . For the forward flow, a rise in  $r/d_s$  will increase the exit cross-sectional area  $a_{s,o}$ , thus reducing  $k_+$ . Notably, after rounding, even  $r/d_s$  is 0.05,  $k_+$  is larger than  $k_-$ . However, for the case without rounding,  $k_-$  is slightly larger than  $k_+$ , and much larger than that of jet pump with rounding. In the backward flow, for the case without rounding, the restraint at the sharp edge of entrance contracts the flow and the flow separates from the wall. After separation, there will be a difference between the actual flowing area and the cross-sectional area of channel, and the velocity amplitude of the main flow at the exit is much larger than the theoretical value  $a_s u_1 / a_b$ , which eventually leads to the increase in the expansion loss. This can explain why  $k_-$  of the jet pump without rounding is so large. With the rounding, the velocity in the vicinity of the small opening of the jet pump drops significantly and then becomes more uniform along the whole tapered channel.<sup>26</sup> As a result,  $k_-$  decreases visibly after rounding. When  $r/d_s \geq 0.15$ ,  $k_-$  changes slightly. In addition, Re has small influence on  $k_+$  and  $k_-$ , especially for the jet pump with larger  $r/d_s$ .

Similarly,  $k_a$ ,  $k_{\text{total}}$ , and  $\varepsilon$  can be plotted as the functions of  $r/d_s$ , as shown in Fig. 5. For a jet pump without rounding,  $k_a$  is negative, indicating that the pressure drop of the

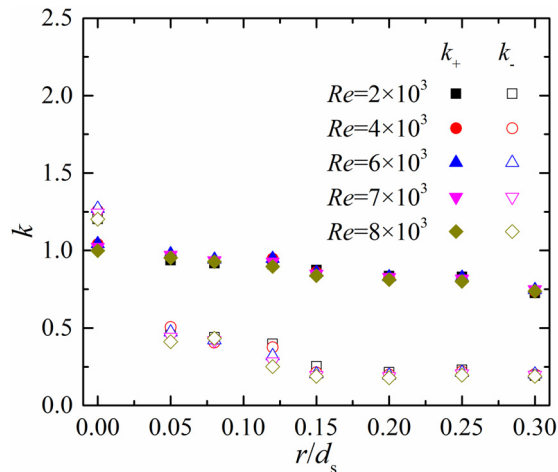


FIG. 4. (Color online) Variations of coefficients of resistance  $k_+$  and  $k_-$  with  $r/d_s$ .

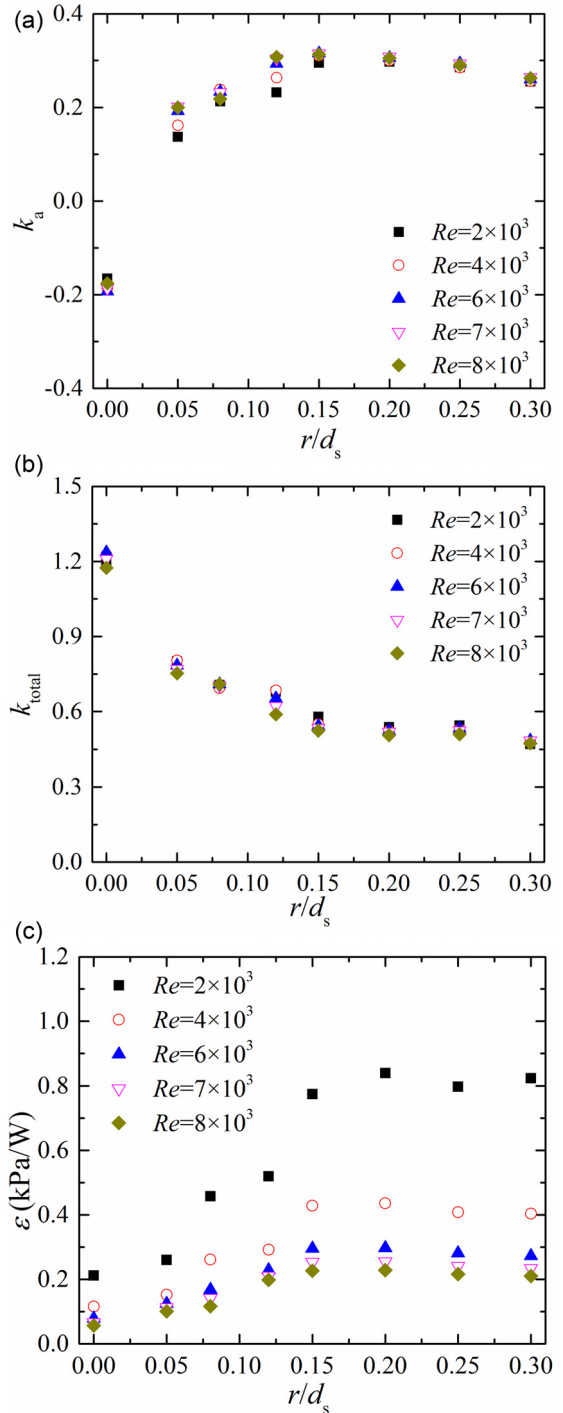


FIG. 5. (Color online) Variations of coefficient of time-averaged resistance  $k_a$  (a), coefficient of overall resistance  $k_{\text{total}}$  (b), and coefficient of effectiveness  $\varepsilon$  (c) with  $r/d_s$ .

forward flow is smaller than that of the backward flow. With rounding at the small opening, even  $r/d_s$  is 0.05,  $k_a$  changes from negative to positive. The time-averaged pressure drop increases with  $r/d_s$  in the converging direction, and when  $r/d_s \geq 0.15$ , it decreases slightly. As can be seen from Fig. 5(b), the total pressure loss decreases significantly with rounding. However, when  $r/d_s \geq 0.15$ , the variation becomes small.

As a result of increasing time-averaged pressure drop and decreasing total pressure loss caused by rounding, the

working efficiency of a jet pump can be effectively improved with a rise in  $r/d_s$ , especially when  $r/d_s$  is less than 0.15, as shown by  $\varepsilon$  in Fig. 5(c). Moreover, for a given  $r/d_s$ ,  $\varepsilon$  decreases as  $Re$  increases. Therefore, to improve the working efficiency, the designed jet pump should be located at a position where the fluid velocity is small.

### B. Effect of taper angle

The variations of  $k_+$  and  $k_-$  with taper angle  $\alpha$  are depicted in Fig. 6 (Nos. 8–14 in Table I). For a jet pump with the fixed opening areas,  $\alpha$  depends on the length of the jet pump  $L_{jp}$ . Within the taper angle range of our interest in this study, the pressure drop in the converging direction is mainly determined by the jet pump's opening areas, and in this case,  $k_+$  is insensitive to  $\alpha$ . For the backward flow, when  $\alpha$  ranges from  $3^\circ$  to  $9^\circ$ ,  $k_-$  varies little. However, when  $\alpha$  is larger than  $9^\circ$ ,  $k_-$  increases notably with  $\alpha$ . It can be attributed to the flow separation from the wall as  $\alpha$  becomes larger.<sup>26</sup>

We also investigated the dependences of  $k_a$ ,  $k_{total}$ , and  $\varepsilon$  on  $\alpha$ . As presented in Fig. 7, when  $\alpha$  ranges from  $3^\circ$  to  $9^\circ$ ,  $k_a$ ,  $k_{total}$ , and  $\varepsilon$  change slightly with  $\alpha$ , which are determined by the opening areas of both channel ends. Specifically,  $k_a$  and  $\varepsilon$  are larger, and  $k_{total}$  is smaller, which means the jet pump can induce a larger time-averaged pressure drop with a higher working efficiency with  $\alpha$  in the range from  $3^\circ$  to  $9^\circ$ . However, as  $\alpha$  increases beyond  $9^\circ$ ,  $k_a$  and  $\varepsilon$  reduce distinctly, whereas  $k_{total}$  increases, showing noticeable performance degradation. In these cases, the performance of the jet pump is not only affected by the opening areas of both channel ends, but also affected by  $\alpha$ .

### C. Effect of cross-sectional area ratio

As mentioned before, when  $\alpha$  ranges from  $3^\circ$  to  $9^\circ$ , the time-averaged pressure drop are determined by the opening areas of both ends, and the jet pump has a relatively higher performance. In this section, the influence of cross-sectional area ratio  $a_b/a_s$  on the performance of jet pump is discussed for the jet pumps with the taper angle from  $5^\circ$  and  $9^\circ$  (Nos. 8, 11, 15–22 in Table I). Figure 8 presents the variations of  $k_+$  and  $k_-$  with  $a_b/a_s$ . For the forward flow,  $k_+$  decreases

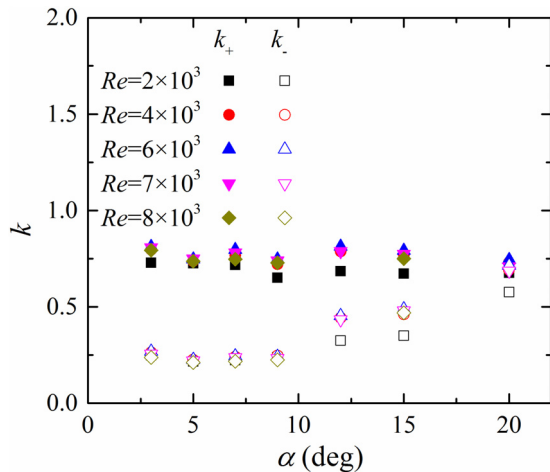


FIG. 6. (Color online) Variations of coefficients of resistance  $k_+$  and  $k_-$  with  $\alpha$ .

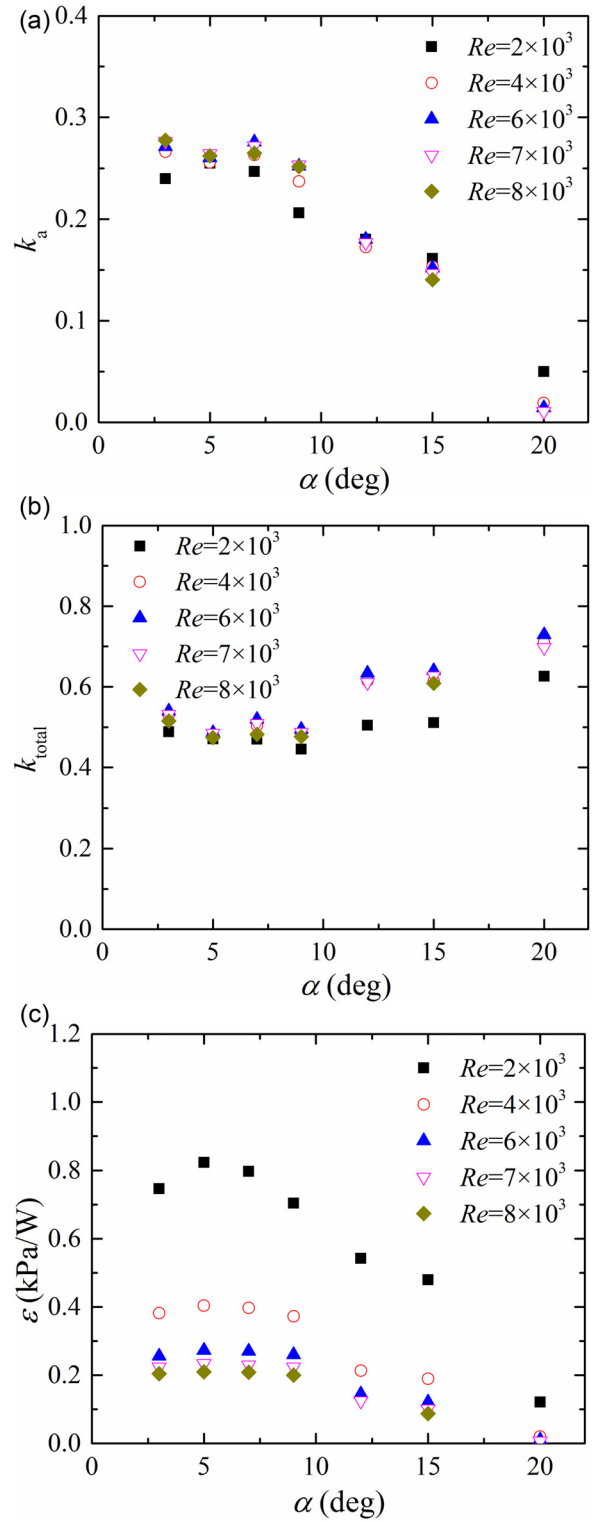


FIG. 7. (Color online) Variations of coefficient of time-averaged resistance  $k_a$  (a), coefficient of overall resistance  $k_{total}$  (b), and coefficient of effectiveness  $\varepsilon$  (c) with  $\alpha$ .

with increasing  $a_b/a_s$ , but the variation is small, as shown in Fig. 8(a). In the backward direction,  $k_-$  drops significantly with a rise in  $a_b/a_s$ , and then reaches a plateau when  $a_b/a_s$  is beyond 2.3. In this study, we vary  $a_b/a_s$  by changing  $a_b$ , while keeping  $a_s$  fixed. For the forward flow through a jet pump in the converging direction,  $a_b$  is the channel inlet opening area, i.e., the compression area, thus increasing  $a_b$  can reduce the

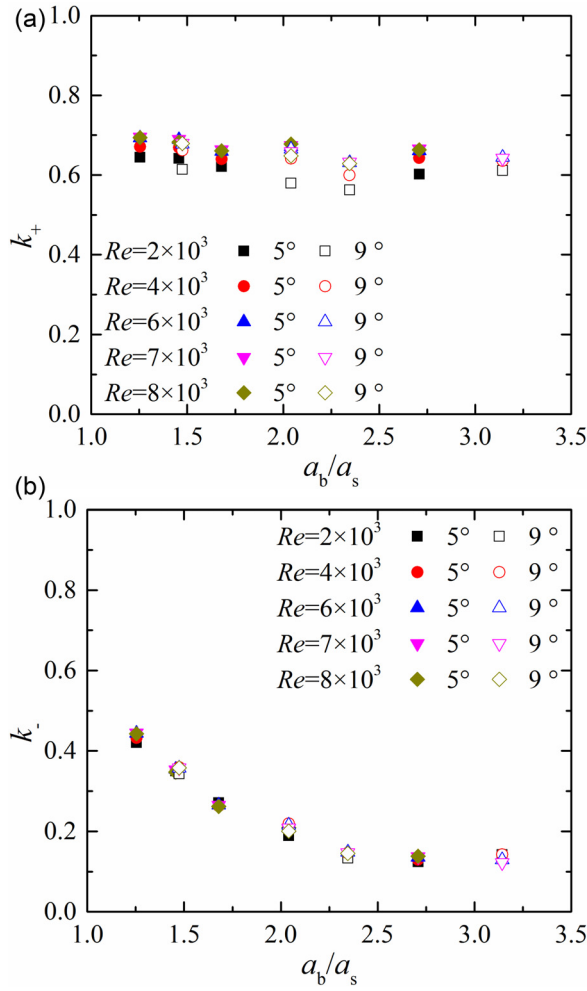


FIG. 8. (Color online) Variations of coefficients of resistance  $k_+$  (a) and  $k_-$  (b) with  $a_b/a_s$ .

compression loss at the channel inlet. This is the reason for the decreasing  $k_+$  with  $a_b/a_s$ . For the backward flow, when  $\alpha$  is less than  $9^\circ$ , the main flow does not separate from the wall, implying the actual flowing area of outlet is closed to the channel outlet opening area, i.e., the big opening area  $a_b$ . Therefore, the expansion area of the outlet increases with a rise in  $a_b$ , which can reduce the expansion loss at the channel outlet and leads to the decrease in  $k_-$ . Notably, for the same  $a_b/a_s$ , the behavior of the jet pumps with the taper angle of  $5^\circ$  and  $9^\circ$  are quite similar, especially for the backward direction.

For a given taper angle,  $k_a$  and  $\varepsilon$  increase, and  $k_{\text{total}}$  decreases with a rise in  $a_b/a_s$ ; however, all the variations become small when  $a_b/a_s$  is beyond 2.3, as shown in Fig. 9. The jet pumps with two different taper angles, i.e.,  $5^\circ$  and  $9^\circ$ , have similar performance for the same  $a_b/a_s$ . The results indicate that the time-averaged pressure drop and the working efficiency can be improved by increasing  $a_b/a_s$ , which is mainly due to the decrease of pressure drop in the backward direction with a rise in  $a_b/a_s$ . However, as  $a_b/a_s$  increases further ( $>2.3$ ), such enhancement becomes negligible.

#### D. Comparison

In order to compare the prediction by Backhaus and Swift<sup>10</sup> with our experimental results, Eq. (1) can be rewritten as

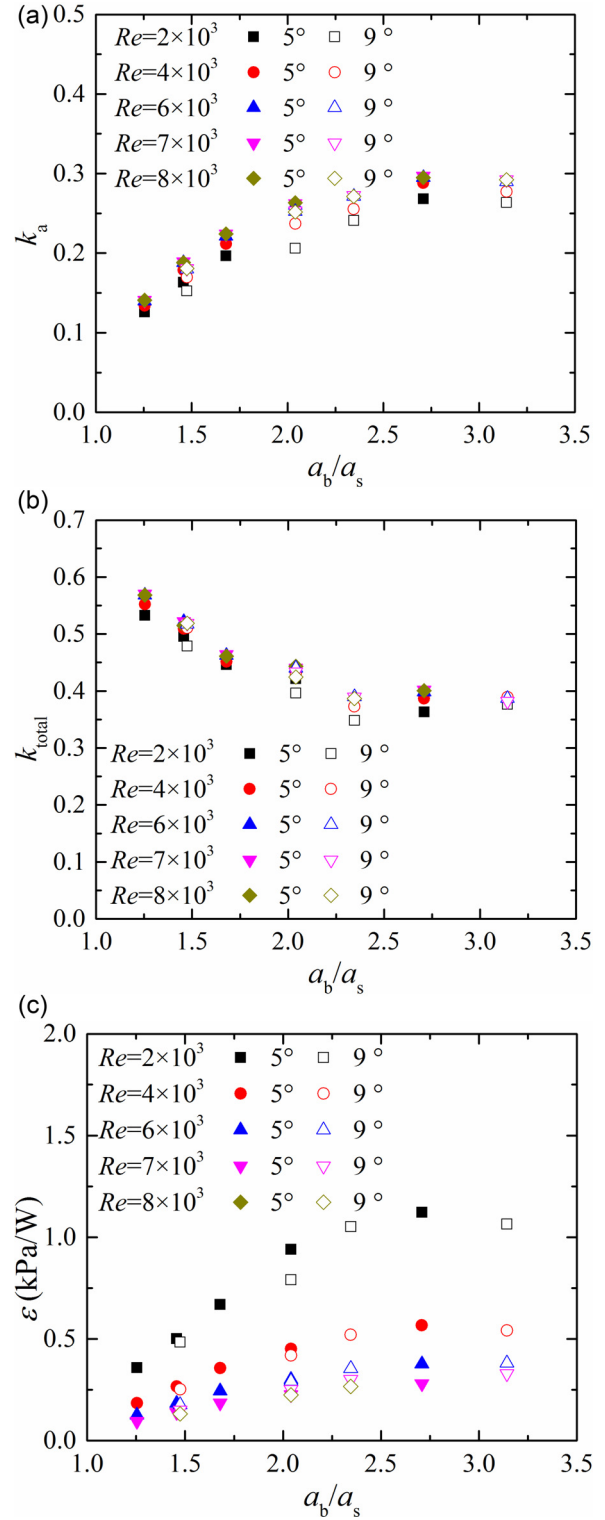


FIG. 9. (Color online) Variations of coefficient of time-averaged resistance  $k_a$  (a), coefficient of overall resistance  $k_{\text{total}}$  (b), and coefficient of effectiveness  $\varepsilon$  (c) with  $a_b/a_s$ .

$$\Delta p_a = \frac{\rho U_{1,jp}^2}{4a_s^2} k_a, \quad (23)$$

$$k_a = \frac{1}{2} \left\{ \left[ k_{\text{exp},s} + \left( \frac{a_s}{a_b} \right)^2 k_{\text{con},b} \right] - \left[ k_{\text{con},s} + \left( \frac{a_s}{a_b} \right)^2 k_{\text{exp},b} \right] \right\}. \quad (24)$$

Equation (24) can be used to calculate  $k_a$  predicted by Backhaus and Swift.<sup>10</sup> Considering  $A_{loop}$  is not much larger than  $a_s$  and  $a_b$  in this study, according to Idelchik's theory,<sup>23</sup>  $k_{exp,s} = (1 - a_s/A_{loop})^2$ ,  $k_{exp,b} = (1 - a_b/A_{loop})^2$ ,  $k_{con,b} = 0.5(1 - a_b/A_{loop})$ , and when  $r/d_s \geq 0.2$ ,  $k_{con} = 0.03$ . Figure 10 compares the calculations by Eq. (24) with the experimental results. From Fig. 10(a), the calculations follow the same trend as the experimental data; that is,  $k_a$  increases and then becomes uniform when  $a_b/a_s$  is larger than a certain value. However, the value of  $k_a$  calculated by Eq. (24) is much larger than the experimental result for a same  $a_b/a_s$ , and the deviation increases with  $\alpha$ , as Fig. 10(b) shows. This comparison implies that Eq. (1) can reflect the impart of  $a_b/a_s$  in the calculation of the time-averaged pressure drop induced by a jet pump. However, the theoretical value overpredicts the time-averaged pressure drop, especially for the jet pump with a larger  $\alpha$ . The reason may be the flow separation for the jet pump with a larger  $\alpha$ , and the imperfect diffuser action even though there is no dramatic flow separation for the jet pump with a smaller  $\alpha$  in the backward flow, which is not included in Eq. (1). This may cause the calculated  $k_-$  to be smaller than the experimental value, and finally lead to the overpredicted  $k_a$  by Eqs. (1) and (24).

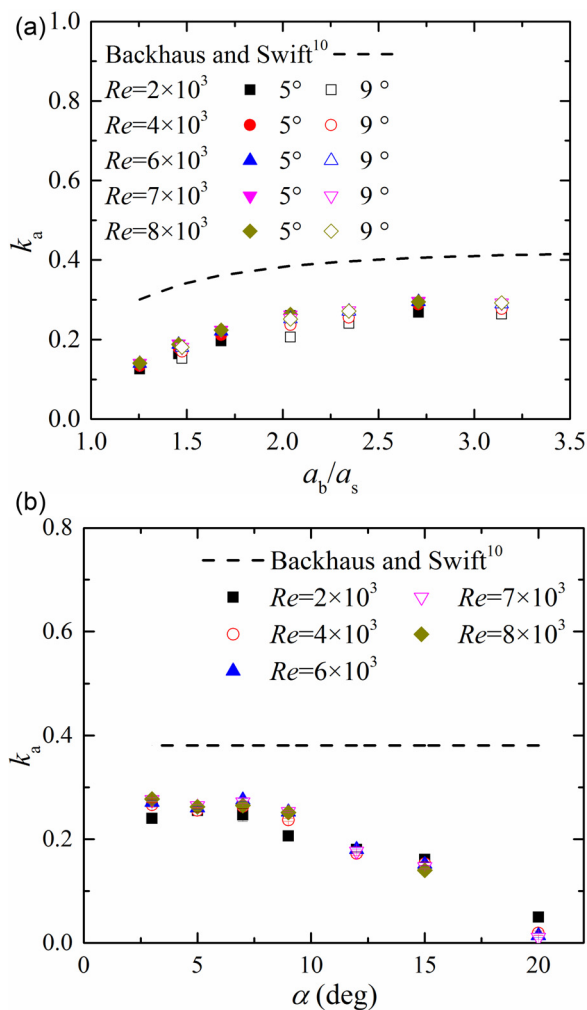


FIG. 10. (Color online) Comparison of calculated results and experimental results for  $k_a$  with  $a_b/a_s$  (a) and  $\alpha$  (b).

## IV. CONCLUSION

In order to study the resistance characteristics of the jet pump in oscillatory flow, an experimental apparatus has been set up to investigate the time-averaged pressure drop induced by the asymmetric flow in the jet pump, as well as its working efficiency. The emphasis is put on the effects of the dimensionless rounding at the edge of the small opening, the taper angle, and the cross-sectional area ratio on the performance of jet pump. The experimental results and the corresponding analyses indicate:

- (1) Rounding the small opening edge can significantly decrease the coefficient of resistance in the backward direction  $k_-$ , which leads to a higher coefficient of time-averaged resistance  $k_a$ , a lower coefficient of overall resistance  $k_{total}$ , and consequently a higher coefficient of effectiveness  $\varepsilon$ . When the dimensionless rounding at the small opening  $r/d_s$  is beyond 0.15, such rounding effect turns out to be small. In addition, a jet pump should be located at the position with smaller flow velocity, which is beneficial to improve the working efficiency of the jet pump.
- (2) When the opening areas of both ends are fixed, jet pumps with the taper angle  $\alpha$  in the range from  $3^\circ$  to  $9^\circ$  are capable of producing a larger time-averaged pressure drop with a higher working efficiency, indicated by the relatively higher coefficient of time-averaged resistance  $k_a$  and coefficient of effectiveness  $\varepsilon$ . However, when  $\alpha$  is larger than  $9^\circ$ , the coefficient of time-averaged resistance  $k_a$  decreases, and the coefficient of overall resistance  $k_{total}$  increases significantly with a rise in  $\alpha$ . This can be attributed to the flow separation from the wall, and the sequent increase of pressure drop in the diverging direction. In addition, when  $\alpha$  ranges from  $3^\circ$  to  $9^\circ$ , the time-averaged pressure drop and working efficiency of a jet pump can be improved by increasing the jet pump's cross-sectional area ratio  $a_b/a_s$ . However, such improvement becomes less prominent when  $a_b/a_s$  increases beyond a certain value.
- (3) Equation (1), proposed by Backhaus and Swift,<sup>10</sup> can present the effect of cross-sectional area ratio  $a_b/a_s$  in the calculation of the jet pump induced time-averaged pressure; however, it will overpredict the time-averaged pressure drop, especially for the jet pump with a larger taper angle  $\alpha$ .

## ACKNOWLEDGMENTS

This work is financially supported by the National Natural Science Foundation of China (Grant Nos. 51376158 and 51576170) and the National Key Research and Development Program (Grant No. 2016YFB0901403).

<sup>1</sup>S. Backhaus, E. Tward, and M. Petach, "Traveling-wave thermoacoustic electric generator," *Appl. Phys. Lett.* **85**, 1085–1087 (2004).

<sup>2</sup>Z. B. Yu, A. J. Jaworski, and S. Backhaus, "Travelling-wave thermoacoustic electricity generator using an ultra-compliant alternator for utilization of low-grade thermal energy," *Appl. Energy* **99**, 135–145 (2012).

<sup>3</sup>Z. H. Wu, L. M. Zhang, W. Dai, and E. C. Luo, "Investigation on a 1 kW traveling-wave thermoacoustic electrical generator," *Appl. Energy* **124**, 140–147 (2014).

- <sup>4</sup>T. J. Bi, Z. H. Wu, L. M. Zhang, G. Y. Yu, E. C. Luo, and W. Dai, "Development of a 5 kW traveling-wave thermoacoustic electric generator," *Appl. Energy* **185**, 1355–1361 (2017).
- <sup>5</sup>S. Hasegawa, T. Yamaguchi, and Y. Oshino, "A thermoacoustic refrigerator driven by a low temperature-differential, high-efficiency multistage thermoacoustic engine," *Appl. Therm. Eng.* **58**, 394–399 (2013).
- <sup>6</sup>L. M. Zhang, J. Y. Hu, Z. H. Wu, E. C. Luo, J. Y. Xu, and T. J. Bi, "A 1 kW-class multi-stage heat-driven thermoacoustic cryocooler system operating at liquefied natural gas temperature range," *Appl. Phys. Lett.* **107**, 033905 (2015).
- <sup>7</sup>C. N. Markides and A. Gupta, "Experimental investigation of a thermally powered central heating circulator: Pumping characteristics," *Appl. Energy* **110**, 132–146 (2013).
- <sup>8</sup>O. A. Oyewunmi, C. J. W. Kirmse, A. J. Haslam, E. A. Müller, and C. N. Markides, "Working-fluid selection and performance investigation of a two-phase single-reciprocating-piston heat-conversion engine," *Appl. Energy* **186**, 376–395 (2017).
- <sup>9</sup>P. H. Ceperley, "A pistonless Stirling engine—The traveling wave heat engine," *J. Acoust. Soc. Am.* **66**, 1508–1513 (1979).
- <sup>10</sup>S. Backhaus and G. W. Swift, "A thermoacoustic-Stirling heat engine: Detailed study," *J. Acoust. Soc. Am.* **107**, 3148–3166 (2000).
- <sup>11</sup>G. Y. Yu, E. C. Luo, W. Dai, and Z. H. Wu, "An energy-focused thermoacoustic-Stirling heat engine reaching a high pressure ratio above 1.40," *Cryogenics* **47**, 132–134 (2007).
- <sup>12</sup>T. Jin, C. S. Mao, K. Tang, H. Zheng, and G. B. Chen, "Characteristics study on the oscillation onset and damping of a traveling-wave thermoacoustic prime mover," *J. Zhejiang Univ. Sci. A* **9**, 944–949 (2008).
- <sup>13</sup>K. de Blok, "Novel 4-stage traveling wave thermoacoustic power generator," in *Proceedings of the Fluids Engineering Division Summer Conference*, Montreal, Canada (August 1–5, 2010), pp. 73–79.
- <sup>14</sup>M. E. H. Tijani and S. Spoelstra, "A high performance thermoacoustic engine," *J. Appl. Phys.* **110**, 093519 (2011).
- <sup>15</sup>A. S. Abduljalil, Z. B. Yu, and A. J. Jaworski, "Design and experimental validation of looped-tube thermoacoustic engine," *J. Therm. Sci.* **20**, 423–429 (2011).
- <sup>16</sup>D. Gedeon, "DC gas flows in Stirling and pulse tube cryocoolers," in *Cryocoolers 9*, edited by R. G. Ross, Jr. (Plenum Press, New York, 1997), pp. 385–392.
- <sup>17</sup>V. Gusev, S. Job, H. Baillet, P. Lotton, and M. Bruneau, "Acoustic streaming in annular thermoacoustic prime-movers," *J. Acoust. Soc. Am.* **108**, 934–945 (2000).
- <sup>18</sup>G. Y. Yu, E. C. Luo, W. Dai, and J. Y. Hu, "Study of nonlinear processes of a large experimental thermoacoustic–Stirling heat engine by using computational fluid dynamics," *J. Appl. Phys.* **102**, 074901 (2007).
- <sup>19</sup>T. Biwa, Y. Tashiro, M. Ishigaki, Y. Ueda, and T. Yazaki, "Measurements of acoustic streaming in a looped-tube thermoacoustic engine with a jet pump," *J. Appl. Phys.* **101**, 064914 (2007).
- <sup>20</sup>K. Tang, Y. Feng, T. Jin, S. H. Jin, M. Li, and R. Yang, "Effect of Gedeon streaming on thermal efficiency of a travelling-wave thermoacoustic engine," *Appl. Therm. Eng.* **115**, 1089–1100 (2017).
- <sup>21</sup>P. Yang, Y. W. Liu, and G. Y. Zhong, "Prediction and parametric analysis of acoustic streaming in a thermoacoustic Stirling heat engine with a jet pump using response surface methodology," *Appl. Therm. Eng.* **103**, 1004–1013 (2016).
- <sup>22</sup>M. Iguchi, M. Ohmi, and K. Meagawa, "Analysis of free oscillatory flow in a U-shaped tube," *Bull. JSME* **25**, 1398–1405 (1982).
- <sup>23</sup>I. E. Idelchik, *Handbook of Hydraulic Resistance*, 3rd ed. (Begell House, New York, 1996).
- <sup>24</sup>A. Petculescu and L. A. Wilen, "Oscillatory flow in jet pumps: Nonlinear effects and minor losses," *J. Acoust. Soc. Am.* **113**, 1282–1292 (2003).
- <sup>25</sup>J. P. Oosterhuis, S. Bühler, T. H. van der Meer, and D. Wilcox, "A numerical investigation on the vortex formation and flow separation of the oscillatory flow in jet pumps," *J. Acoust. Soc. Am.* **137**, 1722–1731 (2015).
- <sup>26</sup>K. Tang, Y. Feng, S. H. Jin, T. Jin, and M. Li, "Performance comparison of jet pumps with rectangular and circular tapered channels for a loop-structured traveling-wave thermoacoustic engine," *Appl. Energy* **148**, 305–313 (2015).
- <sup>27</sup>K. Tang, Z. J. Huang, T. Jin, and G. B. Chen, "Influence of acoustic pressure amplifier dimensions on the performance of a standing-wave thermoacoustic system," *Appl. Therm. Eng.* **29**, 950–956 (2009).
- <sup>28</sup>B. L. Smith and G. W. Swift, "Power dissipation and time-averaged pressure in oscillatory flow through a sudden area change," *J. Acoust. Soc. Am.* **113**, 2455–2463 (2003).
- <sup>29</sup>M. Ohmi and M. Iguchi, "Critical Reynolds number in an oscillating pipe flow," *Trans. Jpn. Soc. Mech. Eng. B* **25**, 165–172 (1982).